Published OnlineFirst October 31, 2016; DOI: 10.1158/1078-0432.CCR-16-1400

Clinical Cancer Research

Simultaneous *In Vivo* Fluorescent Markers for Perfusion, Protoporphyrin Metabolism, and EGFR Expression for Optically Guided Identification of Orthotopic Glioma

Jonathan T. Elliott[1], Kayla Marra[1], Linton T. Evans[2], Scott C. Davis[1], Kimberley S. Samkoe[3], Joachim Feldwisch[4], Keith D. Paulsen[1], David W. Roberts[2], and Brian W. Pogue[1]

Abstract

Purpose: While extent of tumor resection is an important predictor of outcome in glioma, margin delineation remains challenging due to lack of inherent contrast between tumor and normal parenchyma. Fluorescence-guided surgery is promising for its ability to enhance contrast through exogenous fluorophores; however, the specificity and sensitivity of the underlying contrast mechanism and tumor delivery and uptake vary widely across approved and emerging agents.

Experimental Design: Rats with orthotopic F98 wild-type and F98 EGFR-positive ($EGFR^+$) gliomas received *in vivo* administration of IRDye680RD, 5-aminioleuvulinic acid, and ABY-029—markers of perfusion, protoporphyrin metabolism, and EGFR expression, respectively. *Ex vivo* imaging demonstrates the contrast mechanism–dependent spatial heterogeneity and enables within-animal comparisons of tumor-to-background ratio (TBR).

Results: Generally, ABY-029 outperformed PpIX in $F98_{EGFR}$ orthotopic tumor margins and core (50% and 60% higher TBR, respectively). PpIX outperformed ABY-029 in $F98_{wt}$ margins by 60% but provided equivalent contrast in the bulk tumor. IRDye680RD provided little contrast, having an average TBR of 1.7 ± 0.2. The unique spatial patterns of each agent were combined into a single metric, the multimechanistic fluorescence-contrast index (MFCI). ABY-029 performed best in $EGFR^+$ tumors (91% accuracy), while PpIX performed best in wild-type tumors (87% accuracy). Across all groups, ABY-029 and PpIX performed similarly (80% and 84%, respectively) but MFCI was 91% accurate, supporting multiagent imaging when tumor genotype was unknown.

Conclusions: Human use of ABY-029 for glioma resection should enhance excision of $EGFR^+$ tumors and could be incorporated into current PpIX strategies to further enhance treatment in the general glioma case. *Clin Cancer Res; 1–10. ©2016 AACR.*

Introduction

Glioblastoma is the most common primary malignant brain tumor in adults (1), and even when treated aggressively with surgical resection, followed by radiotherapy and/or chemotherapy, median overall survival (OS) remains limited to an average of 16.7 months (2). Along with specific gene expression, Karnofsky Performance Status score and age, extent of tumor resection (EOTR) is a significant predictor of survival duration (3); however, surgeons fundamentally lack adequate visual information during surgery due to poor visual contrast between tumor margins and normal parenchyma. Despite similarities in the gross appearance of malignant tissue and normal brain, there are significant differences in the tumor microenvironment (4), kinetics (5, 6), metabolic activity (7), oxygenation (8), molecular expression (9), and ultrastructure (10) that offer unique sources of exploitable contrast for image-guided surgery. However, exogeneous contrast agents must reach the tumor site to confer tagged contrast, and for this reason, many of these agents are limited by their ability to simultaneously extravasate into tumor margins. An effective imaging agent must exhibit both high extravasation (especially in the tumor margin, where gains in survival are most likely to be realized), and strong mechanisms of contrast between tumor and normal tissue. In this study, fluorescence-guided surgery (FGS) strategies based on vascular permeability, heme biosynthesis metabolism, and tumor-specific cell-surface EGFR overexpression were each compared for their ability to enhance the detection of the glioma tumor boundary in orthotopic models.

Indocyanine green (ICG) is the only widely used imaging agent for FGS, demarcating areas of vascular flow and perfusion (11, 12). However, despite being trusted by surgeons for detecting major blood flow regions, it is a poor choice for brain tumor resection because its mechanism of contrast is based solely on enhanced perfusion and retention (EPR), a weak mechanism of contrast in tumor margins (13). Furthermore, it has very low extravasation in general, due to its high binding affinity to the blood protein albumin (14). Now standard-of-care in Germany for glioma resections, 5-aminoleuvulinic acid–induced protoporphyrin IX exhibits high extravasation across the bulk of tumor regions (2, 15–17); it is also based on strong, and very specific

[1]Thayer School of Engineering, Dartmouth College, Hanover, New Hampshire. [2]Department of Neurosurgery, Dartmouth-Hitchcock Medical Center, Lebanon, New Hampshire. [3]Geisel School of Medicine, Dartmouth College, Hanover, New Hampshire. [4]Preclinical Research, Affibody AB, Solna, Sweden.

Corresponding Author: Jonathan T. Elliott, Thayer School of Engineering, Dartmouth College, 1 Medical Center Dr., 7th Floor, WTRB, Lebanon, NH 03756. Phone: 603-650-1910; Fax: 603 727-7869; E-mail: Jonathan.T.Elliott@dartmouth.edu

doi: 10.1158/1078-0432.CCR-16-1400

Published OnlineFirst October 31, 2016; DOI: 10.1158/1078-0432.CCR-16-1400

Translational Relevance

Fluorescence-guided surgery is emerging as an important tool to improve solid tumor resection; however, the selection of fluorophores that are clinically approved remains limited. Although a number of research groups are developing targeted fluorophores that are more sensitive and specific to tumor cells, it is often unclear how these new enzymatic or immunoactive agents provide value over the currently used blood flow/perfusion agents, such as indocyanine green and the now widely used metabolic marker, 5-aminoleuvulinic acid. In this article, we evaluate a newly developed EGFR-targeted fluorophore, ABY-029 (a candidate for a future exploratory new drug application), by comparing it directly to the clinically used 5-aminoleuvulinic acid and a low-molecular weight perfusion marker in a clinically relevant F98 orthotopic rat tumor model. The findings in this article support the use of ABY-029 in future clinical studies where it has the potential to improve glioma resection rates.

mechanism of contrast, mainly, the tumor-specific downregulation of ferrochelatase (18), which inhibits conversion of excess PpIX that results by the administration of precursor molecule 5-ALA. Unfortunately, 5-ALA FGS is fundamentally limited by weak contrast in low-grade gliomas and in tumor margins. The exact reason for this is controversial, but is likely a combination of decreased extravasation and/or retention, and modulation of enzymes in the heme synthesis pathway (15).

Recently, a unique imaging agent was developed for human use, based on the conjugation of IRDye800CW to a synthesized anti- EGFR Affibody molecule, a ligand selected against the extracellular domain of EGFR. The production name ABY-029 is used to designate the GMP-produced synthetic peptide conjugate which has recently passed toxicity and safety tests in rats (19), as opposed to the functionally equivalent, recombinant protein produced in *E. coli* which is commercially available from Affibody AB for IHC and preclinical experiments, but not suitable for human *in vivo* use. As Affibody molecules are low molecular weight (6.7 kDa) and, in this case, are designed to provide contrast based on EGFR binding, a receptor overexpressed in 50%–70% of brain tumors (20), it is an excellent candidate for image guidance. Furthermore, previous studies have suggested that EGFR is overexpressed in tumor margins (21), providing a potential counterbalance to the decreased extravasation in these important regions. Finally, EGFR is not normally expressed in brain tissue, and therefore, we see that ABY-029 is very specific to tumor cells (22).

In this study, the performance of ABY-029 is compared directly with the 5-ALA–induced PpIX, the emerging clinical standard for fluorescence-guided glioma resection (23), and also to a low-molecular weight permeability tracer, IRDye680RD. A corregistration process was used to compare quantitative contrast values of tumor core, tumor margin, to normal brain regions, across all three imaging agents directly to IHC scores of EGFR and histopathology tumor status. The overall objective was to determine the path forward for augmenting surgical guidance with an optimal combination of agents where feasible, and to investigate the mapping the multiparametric information together to assessing whether they are redundant or synergistic to the resection decisions, based upon pathology evaluation.

Materials and Methods

Cell lines and culture methods

The cell lines used in this study were $F98_{wt}$ (ATCC CRL-2397) and $F98_{EGFR}$ (ATCC CRL-2948), which were ordered from American Type Culture Collection (ATCC) in April, 2015. In addition, $F98_{EGFRvIII}$ cells (ATCC CRL-2949) were obtained in September, 2016, and used in flow cytometry analysis to confirm binding of ABY-029 to a common mutant form of EGFR: variant III (24). Cell lines were cultured at 37°C in DMEM with 10% (v/v) FBS and 1% penicillin–streptomycin. $F98_{EGFR}$ and $F98_{EGFRvIII}$ cells were further selected for by 0.2 mg/mL Geneticin (G418, Thermo Fisher Scientific). Cells were authenticated by ATCC prior to being delivered to Dartmouth, using the short tandem repeat (STR) PCR-based profiling method. $F98_{wt}$ and $F98_{EGFR}$ cells were obtained three months prior to implantation, and in addition to ATCC authentication, were analyzed using flow cytometry before and after implantation to confirm stable cell-surface receptor expression.

Orthotopic Fischer rat glioma model

All animal procedures were conducted according to a protocol approved by the Dartmouth Institutional Animal Care and Use Committee (IACUC) and following best practices set forth by the NIH Guide for Care and use of Laboratory Animals. Rats (*Rattus norvegicus* Fischer 344 strain) were obtained from Charles River Laboratories and housed two-to-a-cage in a biosafety level 2 housing facility on site. A total of 20 female Fischer rats were assigned randomly to one of three groups: $F98_{wt}$ implantation ($n = 8$), $F98_{EGFR}$ implantation ($n = 8$), and SHAM implantation ($n = 4$). The procedure for orthotopic implantation was identical to previous studies (6). Briefly, this involved anesthesia induction by 1%–3% isoflurane, involved the sterotatic injection of 1×10^6 cells in cell culture media using a 25-μL Hamilton syringe (Hamilton Co.) into the cortex 3-mm anterior to the bregma and about 4-mm lateral to the midline, with a depth of approximately 3 mm. SHAM animals received the identical surgical procedure but sterilized PBS was used in lieu of tumor cells. Animals were recovered and monitored during tumor growth until they showed early signs of weight loss, which occurred an average of 21 days postimplantation (range: 13–28 days). Rats weighed on average 147 ± 35 g on the day of imaging.

Production and characterization of pre-GMP ABY-029

The ABY-029 compound was produced by first performing peptide synthesis of anti-EGFR Affibody (Affibody AB) and then performing conjugation with IRDye800CW Maleimide (LI-COR Biosciences, Inc.) Protein synthesis was performed by Bachem AG under guidance from Affibody AB, and the resulting anti-EGFR peptide was given the name Z03115-Cys-trifluoracetate (lot no. 1056475). The purity of the compound was verified by Bachem AG using a reverse-phase rapid HPLC method. No impurities, related substances or degradation compounds, were detected with an abundance of $\geq 0.5\%$. The lyophilized compound was dissolved in DPBS and conjugated to IRDye800CW maliemide at a dye to protein molar ratio of 1.2 to 1. The final ABY-029 compound was recovered by Zeba column filtration at a concentration of 0.33 mg/mL. Fluorescence spectroscopy (Cary 50 UV-Vis,

Published OnlineFirst October 31, 2016; DOI: 10.1158/1078-0432.CCR-16-1400

Varian Medical Systems) and absorption spectroscopy (FluoroMax 3, Horiba Scientific) measurements were acquired from 35 μmol/L samples of ABY-029 and of unlabeled IRDye800CW to evaluate the influence of conjugation on spectral features.

MRI

On the day of the imaging animals were induced with 1%–3% isofluorane before being fitted with an inhalation mask and placed in a custom MR receiver coil. The coil was placed onto the bed of a 3T MRI (Philips Achieva series) and moved into the bore of the magnet. Following a survey image series, which was used to correctly orient the acquisition, precontrast T1- and T2-weighted images were acquired. Gadolinium diethylenetriaminepentacetate (Gd-DTPA, also called gadopentetate dimeglumine; Magnevist, Bayer Schering Pharma) was administered at a dose of 12 mg/kg, and T1 images were acquired at 5 minutes and 15 minutes postinjection.

Fluorescence imaging

During MRI imaging, when the Gd-DTPA contrast (dose of 12 mg/kg) was administered, IRDye680RD (dose of 2.4 μg/kg), ABY-029 (dose of 56.2 μg/kg), and 5-ALA (dose of 75 mg/kg) were also injected simultaneously, as a PBS-diluted solution totaling 800 μL in volume. After MR imaging, animals were recovered and after 3 hours elapsed, the animals were sacrificed, brains were removed, and sectioned into 2-mm slices starting caudally and working towards the nose. In one case, the tumor was evident on the cortical surface, and was imaged before slicing in a planar fluorescence imaging system (Pearl Impulse, LI-COR Biosciences, Inc.). Slices were placed on microscope slides, and imaged first on a GE Typhoon flatbed laser scanner to obtain fluorescence intensity images of PpIX, at 50 μm pixel resolution using 633 nm excitation laser and a 650 nm long pass emission filter. After imaging PpIX, the slides were placed on the Odyssey CX-I (LI-COR Biosciences) flatbed laser scanner to capture the distribution of ABY-029 and IRDye680RD at 42-μm pixel resolution, using the 800 (785 nm laser source) and 700 (685 nm laser source) emission channels of the system respectively, which are past the Q-band fluorescence of PpIX and therefore do not introduce cross-talk.

Histopathology and immunohistochemistry

Following fluorescence imaging, the slides with tissue sections were stored for 24 hours at −20°C, before being immersed in a 10% formalin solution. The sections, which remained relatively well intact, were then placed in small plastic cassettes and sent to the histopathology department for processing. Formalin-fixed sections were embedded in paraffin blocks, faced, and sliced in 4-μm thickness, and mounted on Leica microscope slides. Hematoxylin and eosin (H&E) staining was performed on each block. For IHC, the Leica Bond Rx Automated Stainer (Leica Microsystems, Inc.) protocol was followed: first, the slides were baked for 30 minutes and dewaxed with Leica Bond Dewax solution (ar9640, Leica). Antigen retrieval was performed at a pH 9.0 solution for 20 minutes. The EGFR primary antibody was diluted 1:300 and incubated on the tissue for 15 minutes (ab52894, AbCam) and the Ki67 primary antibody was diluted 1:200 and incubated on the tissue for 15 minutes (crm325a, Biocare). Primary antibody binding was visualized using diaminobenzidine chromogen and a hematoxylin counterstain (DS9800, Leica). The EGFR slides were scored according to the criteria which has been used previously by our group (9): 0, no staining; 1+, partial membranous staining around cells; 2+, weaker membranous staining completely around cells; and 3+, strong membranous staining completely around cells.

Flow cytometry

***Flow cytometric analysis of EGFR expression* in vitro.** To determine the EGFR expression of the $F98_{wt}$, and $F98_{EGFR}$-transfected tumor lines, cells were trypsinized and resuspended at a concentration of 5×10^5 cells per tube. Cells were first labeled with EGF Biotin-XX Conjugate (4 ug/mL, Thermo Fisher Scientific), followed by a secondary antibody Cy5 Streptavidin (40 μg/mL, Thermo Fisher Scientific). Control tubes were stained with secondary antibody only (both positive and control tubes were performed in triplicate). Flow cytometric data were acquired with a FACSCalibur analysis system equipped with a FACStation, and Cell Quest Acquisition software (Becton Dickinson). Fluorescence was quantified using Quantum Cy5 MESF beads, as described by the manufacturer (Bangs Laboratories, Inc.). The number of EGF receptors per cell was calculated assuming one molecule of biotin per EGF and three Cy5 fluorophores per streptavidin molecule, as specified by the manufacturer.

***Flow cytometric analysis of ABY-029 binding* in vitro.** $F98_{wt}$, $F98_{EGFR}$, and $F98_{EGFRvIII}$ cells were trypsinized and resuspended as described above and incubated with 4.74 μg/mL ABY-029. To determine cell viability, a Live/Dead Assay Kit was used (cat# L3224, Thermo Fisher Scientific) such that 2 μL 50 μmol/L ethidium homodimer-1 and 4 μL 2 mmol/L calcein AM were added to the appropriate tubes. Cells were stained with all three dyes, each dye alone, and no dye as a negative control (each group was performed in triplicate). Data were obtained using a MacsQuant 10 Flow Cytometer.

Image coregistration and selection of comparison points

A multistep image registration procedure was developed in-house and applied to the data to enable spatial comparisons at a fine resolution. The fluorescence data acquired on the Odyssey and Typhoon were corregistered to each other by image resizing according to the pixel resolution defined during image acquisition, applying a binary mask and minimizing the difference between images through translation and rotation. Following colocalization of fluorescence image data, histopathology images were registered to the fluorescence data in the following steps. First, the boundary of the tissue slices were identified by having the user manually window and level the image until the tissue section appeared black and the background white. The positive space was identified by having the user draw a line segment from the background to the foreground, and the function *bwtraceboundary* was used to identify the boundary. Second, structural landmarks were selected in both the histology and fluorescent images to serve as control points for an affine transformation, using the matlab function *fitgeotrans*. The transformation matrix was applied to the histology image using *imwarp*, and the control points and boundary x,y points were shifted according to the transformation by *tformfwd*. The tumor was manually segmented by the user, and the center of mass of the tumor identified. Lines were drawn from the center of the tumor outward in all directions, spaced 12 degrees apart, and the intersection of the lines and the boundary were identified. This was done in both the histology and fluorescence image. These points were used as control points for a

Published OnlineFirst October 31, 2016; DOI: 10.1158/1078-0432.CCR-16-1400

B-spline non-rigid transformation, performed using an open source MATLAB package from the MathWorks File Exchange (25). The impetus for selecting the center of the tumor mass is the observation that non-rigid deformation occurs during the formalin fixation process due to the difference in fluid content of the tumor. The B-spline control points were applied to the histology image and also to the binary masks representing the tissue slice boundary and the tumor boundary. An additional region-of-interest representing the tumor margin was created from the 480-μm peripheral aspect of the tumor region-of-interest using the *imerode* function. Ten regions of interest 1.5 mm^2 in area were selected from the background, margin, and tumor core regions randomly, enabling objective comparisons of fluorescence and IHC variables from regions identified independently from histopathology images.

Statistical and image analysis

Group averages were analyzed for main effects using ANOVA with *post hoc t* testing using Bonferroni corrections, to assess the validity of differences between groups where a single condition changed. As Pearson coefficient is valid only when comparing two continuous variables, confirmation of a statistically significant correlation between the continuous variable, ABY-029 fluorescence, and the nominal variable of EGFR IHC score was determined using η. Logistic regression analysis was used to determine the relationship between continuous-independent variables and continuous or ordinal-dependent variables. Multivariate logistic regression was performed to determine the relationship between the binary variable, tissue positivity, and the fluorescence intensity for each dye, and to build conditional model for the multimechanistic fluorescence contrast index (MFCI) probability function. ROC curve analysis was performed to determine the accuracy of the three dyes separately, and of the MFCI metric, to differentiate between normal tissue and tumor. All statistical analyses were performed using MATLAB R2015a (The MathWorks) and IBM SPSS Statistics 23 (IBM). An in-house developed visualization software package was used to display overlays and provide perceptually balanced palettes for parametric data colormaps (26).

Results

In vitro ABY029 characterization

Flow cytometry was used to determine EGFR expression *in vitro* for $F98_{wt}$ and $F98_{EGFR}$; $2 \times 10^2 \pm 2 \times 10^2$ EGFR receptors were detected on the $F98_{wt}$ cells, compared with $3 \times 10^4 \pm 2 \times 10^2$ EGFR receptors on the EGFR positive ($EGFR^+$) cells. Next, flow cytometry was used to confirm specific binding of ABY-029 to $F98_{EGFR}$. The difference in fluorescence signal observed when F98 wild-type, $EGFR^+$ and EGFR-vIII-positive cells are incubated with ABY-029 and measured by flow cytometry are shown in Fig. 1A. After removing dead cells and cell fragments using forward and back scatter and a live-dead cell assay, the mean fluorescence intensity of F98 wild-type cells was 4×10^5 RFUs compared with 5×10^8 RFUs for the $EGFR^+$ cells. Flow cytometry was also performed in the same manner on F98 EGFR-vIII–positive cells; the mean fluorescence intensity of these cells was 2×10^8 RFUs.

Spectroscopic properties of ABY-029 were compared with IRDye800CW, the original unconjugated dye used to produce ABY-029. Conjugation of IRDye800CW and anti-EGFR Affibody caused a slight red-shift in absorption and emission spectra of the IRDye800CW component (Fig. 1B). However, this did not affect the relative intensity of the emission, or the overall Stokes shift. The peak absorption of light was 768 nm and 773 nm for IRDye800CW and ABY-029, respectively, and the peak emission of light was 792 nm and 798 nm, respectively.

Uptake and distribution of ABY029, PpIX, and IRDye in orthotopic gliomas

At the onset of symptoms (e.g., weight loss) in rats bearing orthotopic tumors, imaging proceeded promptly. Pre- and post-gadolinum T1 images, and T2-weighted images were acquired in the 3T MRI prior to sacrificing the animals. Figure 2 shows whole brain images acquired with the planar fluorescence imaging device, which were overlaid onto RGB images to simulate a visualization in clinical applications (Fig. 2B and C). The fluorescence intensity hotspot colocalized well with the large mass evident on the contrast-enhanced T1 MRI image taken pre-mortem.

The tumor-to-background ratio (TBR) was calculated for each of the 20 animals at 20 different points (400 points) as shown in Fig. 2; group means for each imaging agent are summarized in Fig. 2D for tumor margin and tumor core regions. ABY-029 showed 1.5-fold higher TBR values in $EGFR^+$ tumor margins, compared with PpIX ($P < 0.05$) and a 1.6-fold higher level of contrast in the tumor core than PpIX ($P < 0.05$). In wild-type tumors, ABY-029 showed significantly less contrast in either the tumor core ($P < 0.001$) or margin ($P < 0.005$), whereas PpIX showed higher contrast in the margin of 3.1 ± 0.3 ($P < 0.05$), but similar levels in the core (2.9 ± 0.2, $P = 0.15$).

Figure 3 shows a series of images acquired on tumor sections of ABY-029, PpIX, and IRDye680RD fluorescence. The first three rows represent F98 $EGFR^+$ tumors. In these sections, ABY-029 shows strong spatial colocalization with EGFR-stained regions, and PpIX enhancement reflects a similar distribution to ABY-029, but is generally more diffuse. Occasionally, PpIX shows accumulations of fluorescence in a double-band pattern, corresponding roughly to the viable tumor core. Consistently, IRDye680 showed strong accumulation in the necrotic core of the tumor, both in

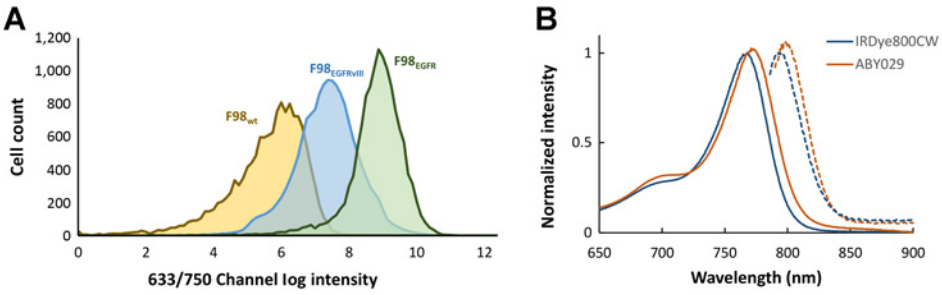

Figure 1.

A, Flow cytometry results showing the red channel log intensity of $F98_{wt}$, $F98_{EGFR}$, and $F98_{EGFRvIII}$ cells following incubation with ABY-029, selected using a live/dead assay. **B,** Excitation (solid lines) and emission curves (dashed lines) of pure IRDye800CW and of ABY-029, showing the slight red shift caused by conjugation to anti-EGFR Affibody molecules.

Published OnlineFirst October 31, 2016; DOI: 10.1158/1078-0432.CCR-16-1400

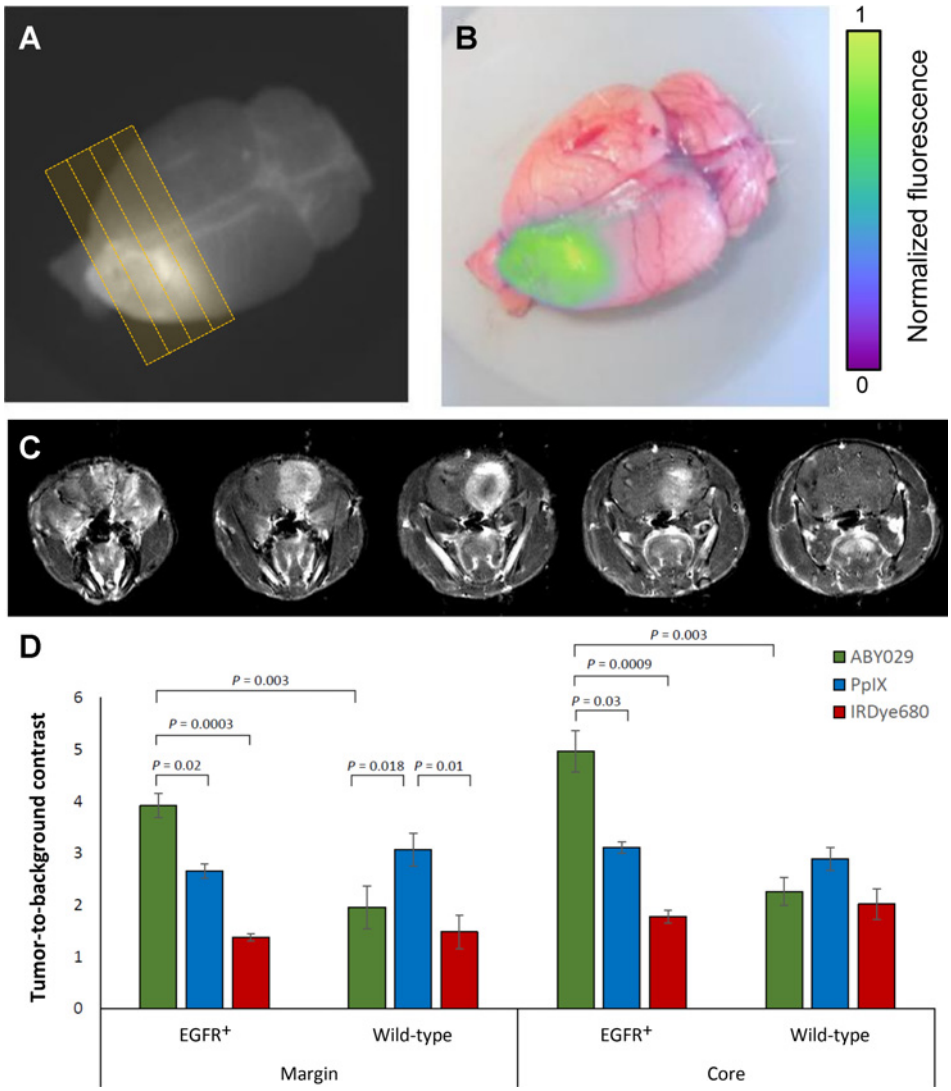

Figure 2.

A, Planar fluorescence image taken 3 hours following injection of ABY-029 and the corresponding RGB overlay (**B**). **C,** A sequence of T1-weighted MRI acquired 15 minutes post-Gd-DTPA injection is visible by planar fluorescence imaging 3 hours following injection of ABY-029 (**B**, raw; **C**, RGB overlay). Red dashed line indicates the MR imaging plane. **D,** Mean tumor-to-background contrast for ABY-029, PpIX, and IRDye680RD in the tumor margin and tumor core, for $F98_{EGFR}$ ($n = 8$) and $F98_{wt}$ ($n = 8$) orthotopic rat glioma tumors.

EGFR-positive and wild-type tumors. IRDye680RD also exhibited background enhancement in certain cases. Often, these regions were coincident with edema. In wild-type animals, tumors are minimally enhanced by ABY-029, but well-enhanced by PpIX. The lack of enhancement is also observed in the EGFR IHC micrographs. Generally, PpIX images seem to contain more high spatial frequency features, sharper edges and patterns, than the ABY-029 images. However, they also seem to exhibit higher background signal than ABY-029. PpIX also appears to be completely lacking enhancement in any necrotic regions, as indicated on H&E micrographs; ABY-029, on the other hand, appears to retain enhancement in these necrotic regions to a greater degree. In general, ABY-029 and PpIX both show a strong ability to delineate the tumor regions indicated by high cell density on the H&E sections. Both show marked differences in spatial distribution, and neither is fully capable of completely enhancing the tumor in a fully specific manner. However, qualitatively, both dyes appear to be useful agents for the purpose of fluorescence-guided surgery, with specific and sensitive patterns of enhancement.

IHC scores correlate with ABY029 intensity

IHC slides stained with EGF antibody consistently reflected the spatial patterns of distribution observed in the ABY-029 fluorescence images. Figure 4 shows a representative example reflecting this pattern similarity. While the fluorescence images lacked the detail provided by the IHC slides, areas of darkest stain corresponded to the hyperintense regions on the fluorescence image. The two regions highlighted by white rectangles on the ABY-029 and PpIX fluorescence images are further magnified (Fig. 4F–K). For each of these, 10× magnified micrographs of H&E, EGFR IHC, and Ki67 IHC are shown. In many cases, EGFR IHC shows strong agreement with Ki67, but EGFR also shows stronger concentration at the invasive margins of the tumor region. To further determine the degree to which EGFR density reflected the fluorescence patterns, five regions-of-interest were randomly selected from 16 different tumor sections (both EGFR positive and wild-type; total 80 ROIs), and given an EGFR score. Figure 4E shows the relationship between these scores and the fluorescence signal in the corresponding

Published OnlineFirst October 31, 2016; DOI: 10.1158/1078-0432.CCR-16-1400

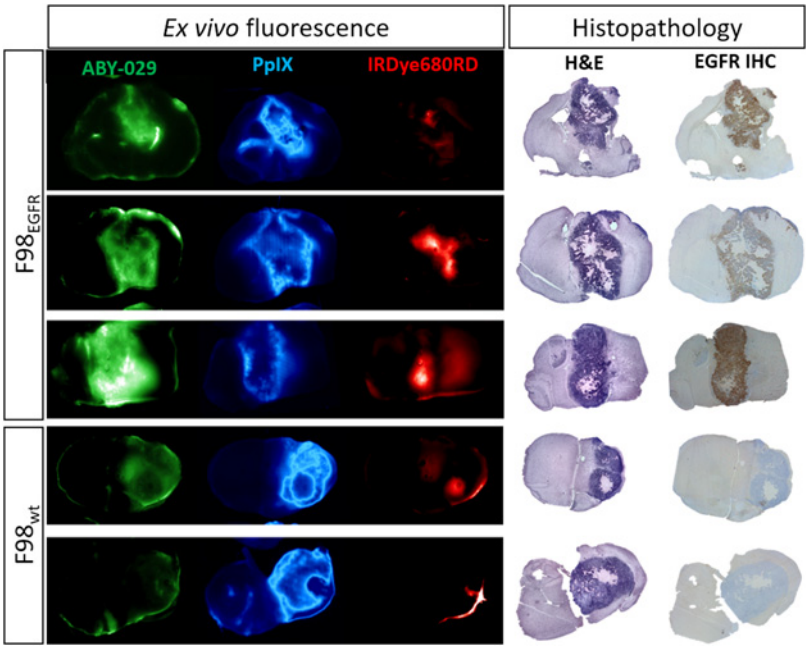

Figure 3.
Ex vivo fluorescence images from animals bearing $F98_{EGFR}$ orthotopic gliomas, acquired 3 hours following coinjection of ABY-029 (green), 5-ALA to induce PpIX (blue), and IRDye680RD (red), and corresponding H&E- and EGFR-stained histopathology images.

ABY-029 image region-of-interest; regression analysis of the relationship between IHC score and fluorescence revealed a strong correlation ($\eta = 0.84$, $P < 0.001$).

Logistical regression and ROC curve analysis

The differential spatial distributions observed in the fluorescence signal of the dyes suggests that important differences in performance exist when using the fluorescence signal to guide tumor resection. The tumor probability curves of the three dyes were calculated from the sample points used in the previous sections, stratified by $EGFR^+$ status. Only ABY-029 showed a significantly different tumor probability curve ($P < 0.001$) when comparing $EGFR^+$ tumors to wild-type tumors. The maximum true positive rate was reduced to 85% from 99% and the minimum true positive rate was increased from 1% to 6% for ABY-029. The PpIX true positive rates ranged from 2% to 99% across the

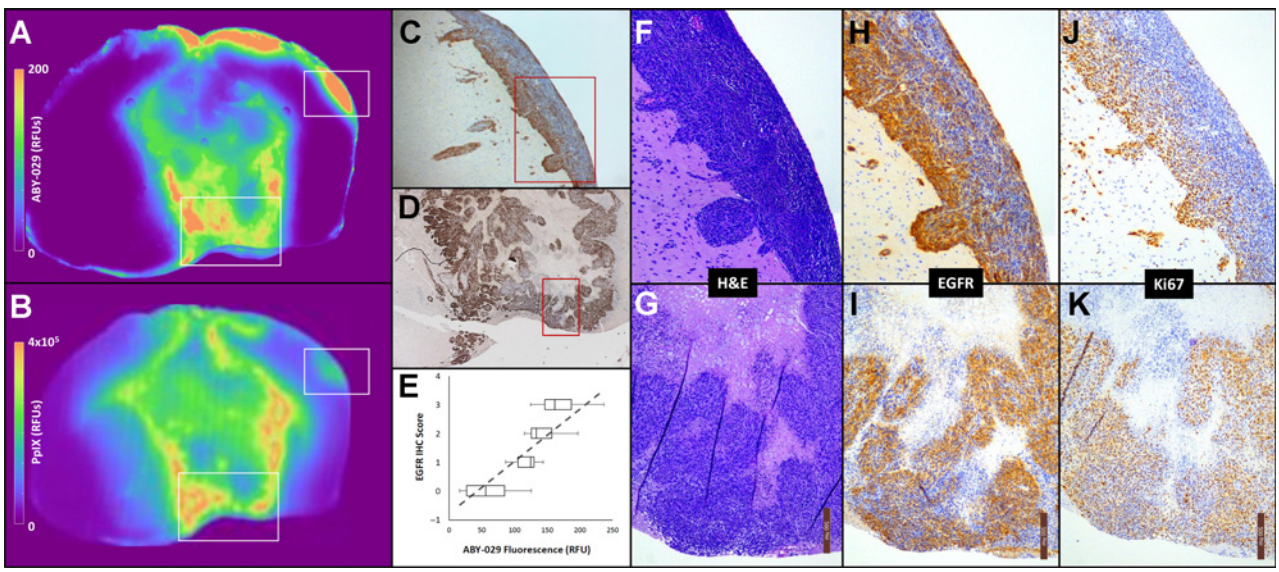

Figure 4.
A, A color map representation of the ABY-029 fluorescence signal and PpIX fluorescence signal in an $F98_{EGFR}$ tumor (**B**). Strong spatial agreement between ABY-029 fluorescence and EGFR-stained IHC images were observed in the tumor core (**D**) and at distant regions of tumor invasion (**C**). This pattern similarity is observed across all animals: quantitatively, the variation in intensity showed good agreement with IHC EGFR score by regression analysis ($\eta = 0.84$, $P < 0.001$; **E**). For the regions within **C** and **D** indicated by red squares, higher power micrographs (10×) show the H&E-stained morphology (**F** and **G**), IHC stain for EGFR (**H** and **I**) and the IHC stain for Ki67, a marker of proliferation (**J** and **K**).

Published OnlineFirst October 31, 2016; DOI: 10.1158/1078-0432.CCR-16-1400

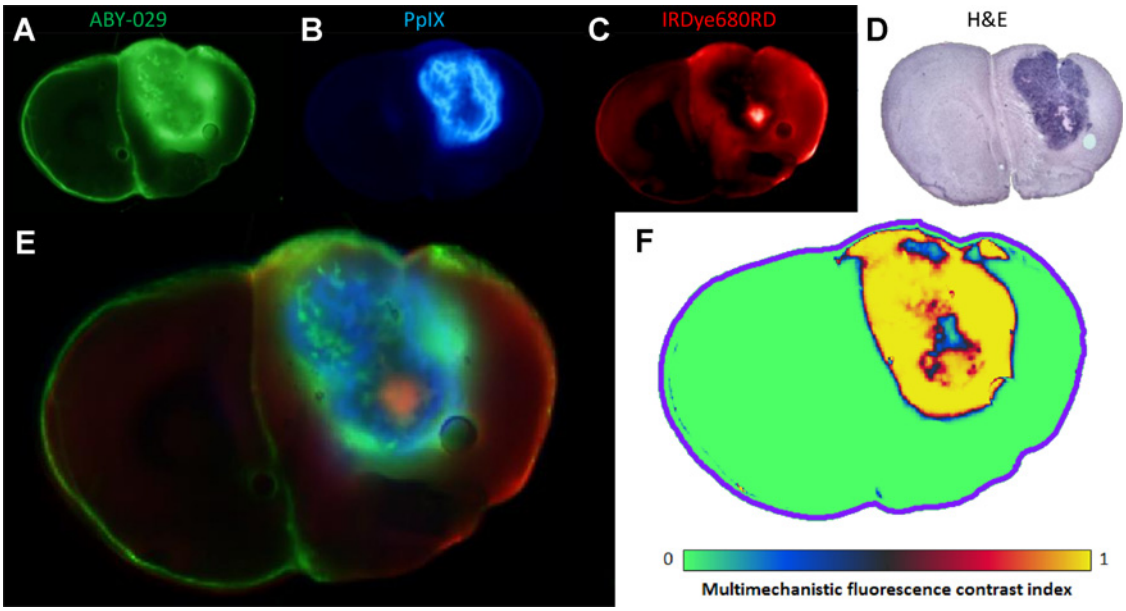

Figure 5.
A representative example of the three imaging agents used in the study, showing the individual fluorescence channels (**A–C**) and the corresponding H&E image (**D**), a composite RGB fluorescence image (**E**), and the tumor probability as predicted by the multimechanistic fluorescence contrast index (MFCI) (**F**).

range of fluorescence values, whereas the maximum true positive rate for IRDye680RD was 80% for both EGFR$^+$ and wild-type tumors. A multiple logistic regression analysis was used to determine the expression mapping the measurement variables combined into a single aggregate metric to tumor positivity status (Fig. 5). This metric, termed the MFCI, is defined as the multivariate logistic regression function with coefficients $\beta_1 = 75.9 \pm 31.7$, $\beta_2 = 11.5 \pm 1.3$, $\beta_3 = 21.6 \pm 5.1$, and $\beta_0 = -14.7 \pm 1.8$.

ROC curve analysis showed marked differences in the performance of the agents within the two tumor lines, in terms of accuracy in differentiating between tumor and normal brain (Table 1). For wild-type tumors, PpIX performed the best, and ABY-029 the worst, of the three agents. In contrast, ABY-029 outperformed the other two agents when only EGFR$^+$ tumors were considered. When the groups were collapsed down to a single pool, ABY-029 and PpIX performed similarly (80% vs. 84% accuracy, respectively), and IRDye680 performed the worst. Interestingly, the MFCI outperformed any of the individual agents in all groups (90% in wild-type tumors, 94% in EGFR$^+$ tumors, and 92% in all sections). A summary of these values, with confidence intervals, can be found in Table 1.

Table 1. Mean accuracy in differentiated between normal brain and tumor, determined by ROC curve analysis, and expressed as a percentage

	Average accuracy (95% CI)		
Agent	**Wild-type**	**EGFR$^+$**	**All sections**
ABY029	69 (67–71)[a]	91 (84–98)[a]	80 (75–85)[a]
PpIX	87 (85–89)	82 (79–85)	84 (83–86)
IRDye680	77 (72–82)[a,b]	75 (69–81)[a,b]	76 (72–80)[a]
MFCI	90 (88–92)[b]	94 (90–98)[a]	91 (89–93)[a,b]

NOTE: The 95% CI of the mean is indicated in the parentheses, and significant differences between the groups, determined by *t* test, are indicated by asterisks.
[a]$P < 0.05$ when compared with PpIX.
[b]$P < 0.05$ when compared with ABY-029.

Discussion

Optimization of contrast enhancement in the context of fluorescence-guided brain surgery is a complex and multidimensional problem. Moreover, the preclinical evaluation of imaging agent performance is fraught with difficulties. For example, the efficacy of imaging agents is often evaluated on the basis of their TBR. However, higher TBR does not correlate with patient outcome unless the tumor margins have contrast, as it is in these important regions where the difference between normal brain and tumor are not easily visualized and incomplete resection is most likely to occur (27). Therefore, it would be advantageous to evaluate imaging agents preclinically, on their performance in both the margins and the solid core of tumors. A challenge to this is that the ability to accurately segment a tissue section image into margin, core tumor, and normal tissue is highly dependent on proper corregistration with histopathology slides. This is a major confounder in many studies evaluating fluorescence guidance, representative sample points are often taken in normal and tumor regions far from the margins (e.g., ref. 28; Fig. 2), and the performance of the imaging agent is overstated. This study addressed this potential confounder in two ways. First, we directly compared the agent of interest, ABY-029, to PpIX and IRDye680 by coinjection and sequential scanning. The result is three channels that are already perfectly corregistered, facilitating comparisons between the agents. To identify tumor margins and core, and to correlate IHC findings, an algorithm was developed to corregister histology slides to the fluorescence data through a series of semiautomated affine and nonrigid deformations, based on control points identified from spatial landmarks. The result is spatial correlation across three fluorescence channels and four IHC slides.

Following proper corregistration, the results of the image analysis demonstrate that the efficacy of ABY-029 is superior to PpIX in both the tumor margin and tumor core for EGFR$^+$ tumors.

Published OnlineFirst October 31, 2016; DOI: 10.1158/1078-0432.CCR-16-1400

As FGS is likely to provide the highest marginal gains at the invasive tumor margins, the improvements in contrast provided by ABY-029 could be substantial. At the tumor margin, the permeability of the blood brain barrier plays a dominant role in the delivery of any contrast administered intravenously; 5-ALA is an extremely small molecule, and therefore likely to be more permeable than IRDye680RD or ABY-029 at these locations. However, the high binding affinity that ABY-029 has for EGFR, coupled with the observed overexpression of EGFR at tumor margins compared with the core, provide a plausible explanation for why ABY-029 showed persistent enhancement comparable with PpIX in the less-permeable margins, despite a moderate difference in molecular weight. Not surprisingly, an entirely different pattern is observed in the $F98_{wt}$ cell line. In these tumors, the absence of EGFR results in a lack of ABY-029 accumulation in the tumor margin. Instead, the spatial pattern mirrors that of IRDye680RD, albeit with somewhat lower concentrations, where contrast is provided by the EPR effect. This finding confirms the specificity of ABY-029's cell-surface receptor mechanism of contrast, which is absent in these tumors. It also suggests that EPR-based contrast is of limited utility in the surgical guidance paradigm, as they provide essentially no contrast in the tumor margins. The relationship between *ex vivo* EGFR expression and *in vivo* ABY-029 accumulation is further highlighted by the correlation observed between EGFR IHC score and fresh tissue ABY-029 fluorescence. As expected, the enhancement patterns of PpIX were not influenced by tissue EGFR status.

One limitation of this study is the availability of only a single time-point which is observable in the destructive, *ex vivo* technique. In the clinical setting, 5-ALA is typically administered 4–8 hours prior to being visualized with the surgical microscope during resection. However, optimal time for administering targeted fluorophores is a topic of debate and varies greatly between different imaging agents. In a preclinical evaluation of the tumor-specific molecule BLZ-100, investigators evaluated *ex vivo* contrast ratios 48 hours following injection (29). Rosenthal and colleagues evaluated the contrast of HER-2–targeted fluorescently labeled antibody on day 3 following infusion (30). Our group is currently performing an evaluation of the optimal timing of imaging; however, preliminary results suggest the highest contrast is obtained between 2 and 6 hours following injection, and that the plasma half-life is approximately 12.5 minutes (data unpublished). Therefore, the timing of the administration of the dyes was selected on the basis of these preliminary results, as well as studies involving 5-ALA administration in tumor-bearing rats which were imaged 2 hours following injection (31). Although the study is somewhat limited by the inability to optimize with certainty the timing of the three dyes, the relative stability of both 5-ALA and ABY-029 at early time points helps to mitigate this confounder. Furthermore, the contrast observed in the 5-ALA measurements, while lower than those observed in human high-grade gliomas, is comparable with previous rat studies which show contrast ratios of between 2:1 and 6:1 (31). All animal models will be limited in their ability to recapitulate human tumor behavior; however, the goal of this article is to perform a direct comparison of the spatial enhancement patterns that would be obtained in a typical neurosurgery timeline with reasonable dye dosing and timing; future work is needed to fully understand the influence of dynamics on intraoperative fluorescence.

Given that ABY-029 and PpIX appear to behave very differently depending on genotype, perfusion, and concurrent therapy, and yet neither agent has perfect accuracy alone, a multivariate logistic regression was performed to describe a combined multimechanistic tumor fluorescence contrast index which is based on the complementarity of the imaging agents. The ROC curve analysis confirms the observation that the spatial differences of the imaging agents across the three groups result in significant differences in accuracy when the fluorescence images are used to differentiate malignant and normal tissue. Furthermore, the logistic regression and ROC curve analyses suggest that ABY-029 and PpIX would be complimentary in a general glioma patient population where EGFR status is unknown prior to surgery, and shows high heterogeneity even in the $EGFR^+$ cases (which represent approximately 50% of high-grade cases). Notwithstanding important regulatory hurdles, it may be advantageous to adopt a paired agent or multiagent strategy, and as the list of approved agents grows, optimization of this selection may be a growing area of interest. Previous studies have suggested that the use of targeted/untargeted imaging agents could be used to control for these differences in perfusion and permeability and recover more specific parameters than fluorescence intensity, such as binding potential or *in vivo* receptor concentration (9, 32, 33). Alternatively, two or more complimentary agents might be interpreted in aggregate through logistic regression, avoiding the need for complex kinetic modeling, on the assumption that covariance is dominated by delivery and therefore, multimechanistic contrast is sensitive to tumor-specific properties.

Molecular-guided surgery is relatively nascent, but is gaining traction by building upon preclinical molecular imaging and drug-targeting studies. The choice of EGFR as a target in this study is based upon a large amount of literature that show overexpression of EGFR in solid tumors, including glioblastoma (~50%), head and neck (~90%), and non–small cell lung (~60%; ref. 34). The $F98_{EGFR+}$ tumors used in this study had levels of EGFR expression similar to moderately expressing low- and high-grade human gliomas (e.g., U251 cells had approximately 1.2× higher signal counts than $F98_{EGFR+}$ when measured on flow cytometry), and ABY-029 also showed good preclinical specificity for a mutated EGFR variant (vIII) found in many tumor cells. (35). The selection of EGFR as a target is also supported by PET-imaging studies, where the anti-EGFR Affibody molecule labeled with Indium-111 has been used to image EGFR expression in murine xenographs (36). However, as the field continues to grow, optimization of probe design and selection of target will be important. For example, fluorescent-labeled mAb targeting VEGFR-1 enabled confocal microscopy imaging of thick fresh-tissue sections containing medulloblastoma and PET-sensitive Affibody molecules targeting HER-2 (also called erbB-2) have been used to image breast cancer (37), and, the exploration of additional targets such as HER-2 and VEGFR-1 and -2 are necessary steps to fully optimize FGS, making it both sensitive and specific for *in vivo* tumor imaging where the immunogenic expression of receptors is not known *a priori*.

Conclusions

Several important conclusions can be made, which will influence the translation of this imaging agent to clinical trials. First, ABY-029 is more specific than PpIX, and more efficacious in the margins, for tumor that are $EGFR^+$. Recent clinical trials suggest that low-grade gliomas do not frequently provide reliable visible PpIX fluorescence during surgery. ABY-029 provides another basis

for tumor-specific contrast, and could be promising as an imaging agent to guide resection of low-grade gliomas where EGFR expression is elevated. Furthermore, notwithstanding the challenging regulatory climate for approval and use of new imaging agents, paired use of PpIX and ABY-029 is also supported by the findings of this article, as they appear to offer complimentary enhancement.

Disclosure of Potential Conflicts of Interest

J. Feldwisch is an employee of and holds ownership interest (including patents) in Affibody AB. No potential conflicts of interest were disclosed by the other authors.

Authors' Contributions

Conception and design: J.T. Elliott, S.C. Davis, K.D. Paulsen, B.W. Pogue
Development of methodology: J.T. Elliott, K. Marra, S.C. Davis, K.D. Paulsen, B.W. Pogue
Acquisition of data (provided animals, acquired and managed patients, provided facilities, etc.): J.T. Elliott, K. Marra, L.T. Evans
Analysis and interpretation of data (e.g., statistical analysis, biostatistics, computational analysis): J.T. Elliott, L.T. Evans, S.C. Davis, D.W. Roberts, B.W. Pogue
Writing, review, and/or revision of the manuscript: J.T. Elliott, K. Marra, S.C. Davis, K.S. Samkoe, J. Feldwisch, K.D. Paulsen, D.W. Roberts, B.W. Pogue
Administrative, technical, or material support (i.e., reporting or organizing data, constructing databases): K. Marra
Study supervision: B.W. Pogue

Acknowledgments

The authors would like to acknowledge Kimberley Krueger for her assistance in developing and executing MRI sequences used in the study, and Rebecca O'Meara for preparing histopathology and IHC slides. We would also like to thank Jason Gunn and Sally Hull for experimental and project management and administrative support, and Prof. Geoff Luke for his assistance with acquiring bright-field micrographs.

Grant Support

This work has been supported by NIH research grants R01CA109558, R01CA167413 and R01NS052274, as well as a CIHR fellowship award (to J.T. Elliott).

The costs of publication of this article were defrayed in part by the payment of page charges. This article must therefore be hereby marked *advertisement* in accordance with 18 U.S.C. Section 1734 solely to indicate this fact.

Received June 1, 2016; revised September 26, 2016; accepted October 14, 2016; published OnlineFirst October 31, 2016.

References

1. Ostrom QT, Gittleman H, de Blank PM, Finlay JL, Gurney JG, McKean-Cowdin R, et al. American Brain Tumor Association Adolescent and Young Adult Primary Brain and Central Nervous System Tumors Diagnosed in the United States in 2008–2012. Neuro Oncol 2016;18 Suppl 1:i1–i50.
2. Stummer W, Reulen HJ, Meinel T, Pichlmeier U, Schumacher W, Tonn JC, et al. Extent of resection and survival in glioblastoma multiforme: identification of and adjustment for bias. Neurosurgery 2008;62:564–76.
3. Lacroix M, Abi-Said D, Fourney DR, Gokaslan ZL, Shi W, DeMonte F, et al. A multivariate analysis of 416 patients with glioblastoma multiforme: prognosis, extent of resection, and survival. J Neurosurg 2001; 95:190–8.
4. Jain RK. Normalizing tumor microenvironment to treat cancer: bench to bedside to biomarkers. J Clin Oncol 2013;31:2205–18.
5. Schabel MC. A unified impulse response model for DCE-MRI. Magn Reson Med 2012;68:1632–46.
6. Elliott JT, Samkoe KS, Davis SC, Gunn JR, Paulsen KD, Roberts DW, et al. Image-derived arterial input function for quantitative fluorescence imaging of receptor-drug binding in vivo. J Biophotonics 2016;9:282–95.
7. Di Chiro G, DeLaPaz RL, Brooks RA, Sokoloff L, Kornblith PL, Smith BH, et al. Glucose utilization of cerebral gliomas measured by [18F] fluorodeoxyglucose and positron emission tomography. Neurology 1982;32: 1323–9.
8. Ueda S, Roblyer D, Cerussi A, Durkin A, Leproux A, Santoro Y, et al. Baseline tumor oxygen saturation correlates with a pathologic complete response in breast cancer patients undergoing neoadjuvant chemotherapy. Cancer Res 2012;72:4318–28.
9. Samkoe KS, Tichauer KM, Gunn JR, Wells WA, Hasan T, Pogue BW. Quantitative *in vivo* immunohistochemistry of epidermal growth factor receptor using a receptor concentration imaging approach. Cancer Res 2014;74:7465–74.
10. Krishnaswamy V, Elliott JT, McClatchy DM III, Barth RJ Jr, Wells WA, Pogue BW, et al. Structured light scatteroscopy. J Biomed Opt 2014;19:070504.
11. Schaafsma BE, Mieog JS, Hutteman M, van der Vorst JR, Kuppen PJ, Lowik CW, et al. The clinical use of indocyanine green as a near-infrared fluorescent contrast agent for image-guided oncologic surgery. J Surg Oncol 2011;104:323–32.
12. Vahrmeijer AL, Hutteman M, van der Vorst JR, van de Velde CJ, Frangioni JV. Image-guided cancer surgery using near-infrared fluorescence. Nat Rev Clin Oncol 2013;10:507–18.
13. LeRoux PD, Winter TC, Berger MS, Mack LA, Wang K, Elliott JP. A comparison between preoperative magnetic resonance and intraoperative ultrasound tumor volumes and margins. J Clin Ultrasound 1994; 22:29–36.
14. Baker KJ. Binding of sulfobromophthalein (BSP) sodium and indocyanine green (ICG) by plasma alpha-1 lipoproteins. Proc Soc Exp Biol Med 1966;122:957–63.
15. Stummer W, Novotny A, Stepp H, Goetz C, Bise K, Reulen HJ. Fluorescence-guided resection of glioblastoma multiforme by using 5-aminolevulinic acid-induced porphyrins: a prospective study in 52 consecutive patients. J Neurosurg 2000;93:1003–13.
16. Stummer W, Pichlmeier U, Meinel T, Wiestler OD, Zanella F, Reulen HJ. Fluorescence-guided surgery with 5-aminolevulinic acid for resection of malignant glioma: a randomised controlled multicentre phase III trial. Lancet Oncol 2006;7:392–401.
17. Valdes PA, Leblond F, Kim A, Harris BT, Wilson BC, Fan X, et al. Quantitative fluorescence in intracranial tumor: implications for ALA-induced PpIX as an intraoperative biomarker. J Neurosurg 2011;115:11–7.
18. Peng Q, Warloe T, Berg K, Moan J, Kongshaug M, Giercksky KE, et al. 5-Aminolevulinic acid-based photodynamic therapy. Clinical research and future challenges. Cancer 1997;79:2282–308.
19. Samkoe KS, Gunn JR, Marra K, Hull SM, Moodie KL, Feldwisch J, et al. Toxicity and pharmacokinetic profile for single dose injection of ABY-029: a fluorescent anti-EGFR synthetic Affibody molecule for human use. Mol Imag Biol (under review, 2016).
20. Verhaak RG, Hoadley KA, Purdom E, Wang V, Qi Y, Wilkerson MD, et al. Integrated genomic analysis identifies clinically relevant subtypes of glioblastoma characterized by abnormalities in PDGFRA, IDH1, EGFR, and NF1. Cancer Cell 2010;17:98–110.
21. Hoelzinger DB, Mariani L, Weis J, Woyke T, Berens TJ, McDonough WS, et al. Gene expression profile of glioblastoma multiforme invasive phenotype points to new therapeutic targets. Neoplasia 2005;7:7–16.
22. Sexton K, Tichauer K, Samkoe KS, Gunn J, Hoopes PJ, Pogue BW. Fluorescent affibody peptide penetration in glioma margin is superior to full antibody. PLoS One 2013;8:e60390.
23. Pichlmeier U, Bink A, Schackert G, Stummer W, ALA Study Group. Resection and survival in glioblastoma multiforme: an RTOG recursive partitioning analysis of ALA study patients. Neuro Oncol 2008;10:1025–34.
24. Pedersen MW, Meltorn M, Damstrup L, Poulsen HS. The type III epidermal growth factor receptor mutation. Biological significance and potential target for anti-cancer therapy. Ann Oncol 2001;12:745–60.
25. Kroon D-J. B-spline grid, image, and point based Registration. TheMathWorks File Exchange; 2008. Available from: https://www.mathworks.com/matlabcentral/fileexchange/20057.
26. Elliott JT, Dsouza AV, Davis SC, Olson JD, Paulsen KD, Roberts DW, et al. Review of fluorescence guided surgery visualization and overlay techniques. Biomed Opt Express 2015;6:3765–82.

Published OnlineFirst October 31, 2016; DOI: 10.1158/1078-0432.CCR-16-1400

27. Petrecca K, Guiot MC, Panet-Raymond V, Souhami L. Failure pattern following complete resection plus radiotherapy and temozolomide is at the resection margin in patients with glioblastoma. J Neurooncol 2013;111:19–23.
28. Fidel J, Kennedy KC, Dernell WS, Hansen S, Wiss V, Stroud MR, et al. Preclinical validation of the utility of BLZ-100 in providing fluorescence contrast for imaging spontaneous solid tumors. Cancer Res 2015;75:4283–91.
29. Butte PV, Mamelak A, Parrish-Novak J, Drazin D, Shweikeh F, Gangalum PR, et al. Near-infrared imaging of brain tumors using the Tumor Paint BLZ-100 to achieve near-complete resection of brain tumors. Neurosurg Focus 2014;36:E1.
30. Rosenthal EL, Kulbersh BD, King T, Chaudhuri TR, Zinn KR. Use of fluorescent labeled anti–epidermal growth factor receptor antibody to image head and neck squamous cell carcinoma xenografts. Mol Cancer Ther 2007;6:1230–8.
31. Valdes PA, Leblond F, Jacobs VL, Wilson BC, Paulsen KD, Roberts DW. Quantitative, spectrally-resolved intraoperative fluorescence imaging. Sci Rep 2012;2:798.
32. Tichauer KM, Samkoe KS, Gunn JR, Kanick SC, Hoopes PJ, Barth RJ, et al. Microscopic lymph node tumor burden quantified by macroscopic dual-tracer molecular imaging. Nat Med 2014;20:1348–53.
33. Tichauer KM, Samkoe KS, Sexton KJ, Hextrum SK, Yang HH, Klubben WS, et al. *In vivo* quantification of tumor receptor binding potential with dual-reporter molecular imaging. Mol Imaging Biol 2011;14:584–92.
34. Salomon DS, Brandt R, Ciardiello F, Normanno N. Epidermal growth factor-related peptides and their receptors in human malignancies. Crit Rev Oncol Hematol 1995;19:183–232.
35. Wang D, Chen Y, Leigh SY, Haeberle H, Contag CH, Liu JT. Microscopic delineation of medulloblastoma margins in a transgenic mouse model using a topically applied VEGFR-1 probe. Transl Oncol 2012;5:408–14.
36. Tolmachev V, Rosik D, Wallberg H, Sjoberg A, Sandstrom M, Hansson M, et al. Imaging of EGFR expression in murine xenografts using site-specifically labelled anti-EGFR 111In-DOTA-Z EGFR:2377 Affibody molecule: aspect of the injected tracer amount. Eur J Nucl Med Mol Imaging 2010;37:613–22.
37. Sorensen J, Velikyan I, Sandberg D, Wennborg A, Feldwisch J, Tolmachev V, et al. Measuring HER2-receptor expression in metastatic breast cancer using [68Ga]ABY-025 affibody PET/CT. Theranostics 2016;6:262–71.

Published OnlineFirst October 31, 2016; DOI: 10.1158/1078-0432.CCR-16-1400

Clinical Cancer Research

Simultaneous *In Vivo* Fluorescent Markers for Perfusion, Protoporphyrin Metabolism, and EGFR Expression for Optically Guided Identification of Orthotopic Glioma

Jonathan T. Elliott, Kayla Marra, Linton T. Evans, et al.

Clin Cancer Res Published OnlineFirst October 31, 2016.